crystals

MDPI

Article

Effect of Precursors Concentrations on the Photocatalysis Performance Stability of Electrodeposited ZnO Nanorods and Their Robustness in Aqueous Environments

Abdullah S. Alshammari [1,*], Mansour Mohamed [1,2], Ziaul Raza Khan [1], Mohamed Bouzidi [1,3] and Mohamed Gandouzi [1,4]

[1] Department of Physics, College of Science, University of Hail, Hail P.O. Box 2440, Saudi Arabia
[2] Department of Physics, Faculty of Science, Assiut University, Assiut 71516, Egypt
[3] Unité de Recherche sur les Hétéro-Epitaxies et Applications (URHEA), Faculté des Sciences, Université de Monastir, Monastir 5000, Tunisia
[4] Faculté des Sciences de Tunis, Universite de Tunis El Manar, Tunis 1060, Tunisia
* Correspondence: ashammari@uoh.edu.sa

Abstract: ZnO nanostructured materials have been widely utilized in several environmental depollution applications. In the current work, ZnO nanorods were grown using the electrodeposition method with different precursor concentrations. A variation in the dimensions of the nanorods grown with the different precursor concentrations was noticed, as expected. The ability of the fabricated nanorods to remove water pollutants under UV irradiation and their photocatalytic performance stability was also evaluated over a prolonged period of time. Interestingly, the samples grown in different conditions exhibited different capabilities to maintain their morphology and their photocatalytic performance after they were kept in contaminated water for a long time. Moreover, some samples also were found to remain photocatalytically active for approximately 47% longer than other samples. These findings indicate that the performance stability of ZnO nanorods for pollutants removal and their robustness can be greatly improved by controlling their growth parameters, which will favorably impact the use of ZnO nanorods for water-treatment applications and their economic aspects.

Keywords: ZnO nanorods; electrodeposition; photocatalysis performance; water treatment

Citation: Alshammari, A.S.; Mohamed, M.; Khan, Z.R.; Bouzidi, M.; Gandouzi, M. Effect of Precursors Concentrations on the Photocatalysis Performance Stability of Electrodeposited ZnO Nanorods and Their Robustness in Aqueous Environments. *Crystals* **2024**, *14*, 393. https://doi.org/10.3390/cryst14050393

Academic Editors: Zahira El Khalidi, Elisabetta Comini and Abderrahim Moumen

Received: 31 March 2024
Revised: 16 April 2024
Accepted: 20 April 2024
Published: 24 April 2024

1. Introduction

The emerging nanotechnologies offer practical solutions for many issues in various application fields. Many research groups have used nanotechnology to deal with many environmental problems [1,2]. Nanomaterials and their composites have been successfully utilized for environmental monitoring, environmental control, environmental remediation, and environmental improvements [1–6]. Among the various nanomaterials tested, ZnO nanostructures have shown high potential for environmental applications and hold many promises for substantial future improvements [7]. For example, ZnO quantum dots have been employed in the detection of different organic and inorganic environmental pollutants [8]. ZnO nanoparticles with different morphologies and superior photodegradation ability of methylene blue (MB) have also been reported in the literature [9]. A recyclable photocatalyst based on hierarchical ZnO nanoplate–nanowire structures has been prepared and effectively utilized to degrade methyl orange (MO), an environmental pollutant [10]. ZnO one-dimensional nanostructures have also attracted considerable interest for environmental applications due to their excellent physical and chemical properties. These include ZnO nanorods, nanowires, and nanotubes. The high aspect ratio of these nanostructures and the low production costs made them among the most favorable photocatalyst materials for environmental pollutants degradation [11]. Photodegradation of methylene blue (MB) has been demonstrated with good degradation efficiency using electrodeposited ZnO nanorods [12]. In addition to the important investigations into the properties of these nanostructures and their ability to provide solutions to environmental issues, the recyclability

and the related economic context of ZnO nanostructures in terms of their production costs and durability are equally important. Long ZnO nanowires have been grown and have been utilized in the photodegradation of rhodamine B and 4-chlorophenol. The grown nanowires have shown decent photocatalytic activity, with high potential for use as effective recyclable photocatalysts. ZnO nanoparticles have also been synthesized and tested for rhodamine B degradation. The synthesized nanoparticles have demonstrated a good photocatalytic performance in a number of degradation cycles [13,14]. Moreover, the effect of the type of precursor used to grow ZnO nanocatalysts on their morphological, structural, and photocatalytic properties has been addressed in the literature. ZnO nanostructures prepared using zinc acetate have been shown to have better photocatalytic activity than that prepared using zinc nitrate due to their crystalline quality and specific surface area, according to a previous study [15]. Another study investigated the effect of using different concentrations of the same zinc precursor on the properties of ZnO nanoparticles and reported an improvement in the degradation ability of dyes [16]. Zhang et al. have examined the influence of the aspect ratio of ZnO nanorods on their photocatalytic performance and concluded that increasing the aspect ratio of the nanorods considerably enhances their photocatalytic activity [17]. The shape of ZnO nanostructures also plays a major role in determining their physical properties and photocatalytic performance for environmental applications [18,19]. However, it is well known that erosion of ZnO structures takes place when they are exposed to water, especially water with extreme PH values [20–22]. Therefore, in the field of environmental application and, specifically, water pollutants removal, the stability of the ZnO photocatalysts and their erosion resistance are of great importance in terms of their durability, as well as their economic feasibility for treating contaminated water. Various studies have reported the effect of erosion on ZnO structures for growth orientation and structures transformation in water-splitting and in water-treatment applications [20–27]. Additionally, some previous studies have reported that ZnO shows good thermodynamic stability in aqueous solutions in the high pH range from 8 to 13 [28]. However, it is difficult to find any reports on improving the erosion resistance of ZnO nanostructures in aqueous media through controlling their growth conditions. Therefore, in the current study, we attempt to investigate the effect of the growth conditions on the photocatalytic activity of ZnO nanorods and their water-treatment performance stability. The study also examines the influence of controlling the precursors' concentrations on the erosion resistance of ZnO nanorods in aqueous media and the related morphological changes, along with their correlation with the nanorods' photocatalytic activity durability and their photocatalytic performance stability. The findings of the study are expected to contribute significantly to the ZnO-based nanomaterials research and open the door for further investigations into the production of highly durable, economically feasible, and environmentally friendly water-pollutants removal materials.

2. Materials and Methods

The growth of the ZnO nanorods in this study was carried out using an electrodeposition technique. The electrodeposition method is a low-cost and flexible technique that allows the nanostructured materials to be deposited on a variety of conductive substrates. A simple home-made electrodeposition setup containing a two-electrode cell and a DC power supply was used for the deposition of the nanorods. The working electrode (gold-coated glass substrate) and the counter electrode (platinum wire) were separated by 30 mm during the electrodeposition process. The nanorods were grown on gold electrodes sputtered onto glass substrate with a gold area of 1 cm^2 and a thickness of about 120 nm. Zinc nitrate hexahydrate ($Zn(NO_3)_2 \cdot 6H_2O$, reagent-grade, 98%, from Sigma Aldrich, Gillingham, UK) along with hexamethylenetetramine (HMTA, puriss. p.a. reagent-grade, ≥99.5%, from Sigma Aldrich, UK) were used as precursors and were dissolved in DI water at different molarities in the range from 0.015 M to 0.045 M. The growth solution was kept under continuous stirring and its temperature was gradually raised to 80 °C. Once the temperature stabilized, the gold electrodes were immersed in the growth solution and a voltage of

−1.0 volts was applied. After a period of 1 h, the ZnO nanorods grown on the cathode electrode were removed from the solution and were cleaned with DI water several times and were then dried with nitrogen. Table 1 shows the details of the grown nanorods samples used in this study. The grown nanorods were used to remove methylene blue (MB), an organic pollutant, from water. To achieve this, water samples polluted with 10^{-5} M of MB and with a pH value close to neutral (pH~6.8) were prepared. Each nanorods sample was immersed in a beaker containing 10 mL of the contaminated water and was exposed to a UV light of a power density of 50×10^{-6} W/cm^2 and a wavelength of 365 nm to study the photocatalytic activity of the prepared samples. The UV light source was kept at 10 cm above the tested samples during irradiation. The absorption spectra of the water samples were taken at different times in the range from 0 to 225 min using a Thermo Scientific spectrophotometer (Evolution 300 UV–Vis, Waltham, MA, USA) to evaluate the degradation of the MB with the irradiation time. The samples were also kept in the water for 60 days and their photocatalytic activity was re-evaluated every 30 days to test the performance stability of the prepared samples. Additionally, images of the samples were taken using the FEI Quanta 250 scanning electron microscope to investigate the possible morphological changes in the samples after they had been kept in an aqueous environment for a prolonged period. The variation in the samples' performance in terms of pollutant degradation and in their morphology was analyzed in detail and is presented in the following sections.

Table 1. ZnO nanorods growth details.

Sample	Zinc Nitrate Concentration (M)	HMTA Concentration (M)	Molarity Ratio ZN/HMTA	Growth Temperature (°C)	Applied Potential (V)	Growth Time (min)
S1	0.03	0.015	2.00	80	−1.0	60
S2	0.03	0.045	0.67	80	−1.0	60
S3	0.03	0.03	1.00	80	−1.0	60
S4	0.045	0.03	1.50	80	−1.0	60
S5	0.015	0.03	0.50	80	−1.0	60

3. Results and Discussion

The SEM images of the grown ZnO nanorods samples with different precursor concentrations are shown in Figure 1a. It is clear that the concentration of the precursors strongly affects the growth of the nanorods. Samples prepared from solutions with less HMTA molarity in comparison with zinc nitrate (i.e., S1 and S4) show enhanced growth, with larger nanorods dimensions.

In contrast, samples grown from solutions with more HMTA molarity in comparison with zinc nitrate (i.e., S2 and S5) show nanorods with smaller dimensions. In both situations, the prepared samples have high densities of ZnO nanorods. The sample, S3, prepared from a solution with equal zinc nitrate and HMTA molarities shows successful growth of randomly oriented nanorods with less density and average dimensions in comparison with other samples. These observations confirm the key effect of the precursors concentration on the growth process and the role of a high HMTA concentration in inhibiting the growth of the nanorods. Similar effects have been observed in previous studies [29–31]. The radial growth of the nanorods and the development of their sides is strongly inhibited by the high concentration of HMTA [29].

The following chemical reactions illustrate the role of each precursor, zinc nitrate ($Zn(NO_3)_2$ and HMTA($C_6H_{12}N_4$), in the growth of the ZnO nanorods [29]:

$$Zn(NO_3)_2 \rightarrow Zn^{2+} + 2NO_3^- \quad (1)$$

$$NO_3^- + H_2O + 2e^- \rightarrow NO_2^- + 2OH^- \quad (2)$$

$$C_6H_{12}N_4 + 6H_2O \rightleftharpoons 6COH_2 + 4NH_3 \quad (3)$$

$$NH_3 + H_2O \rightleftharpoons NO_4^+ + OH^- \quad (4)$$

$$Zn^{2+} + 2OH^- \rightarrow Zn(OH)_2 \quad (5)$$

$$Zn(OH)_2 \overset{80^\circ}{\rightarrow} ZnO + H_2O \quad (6)$$

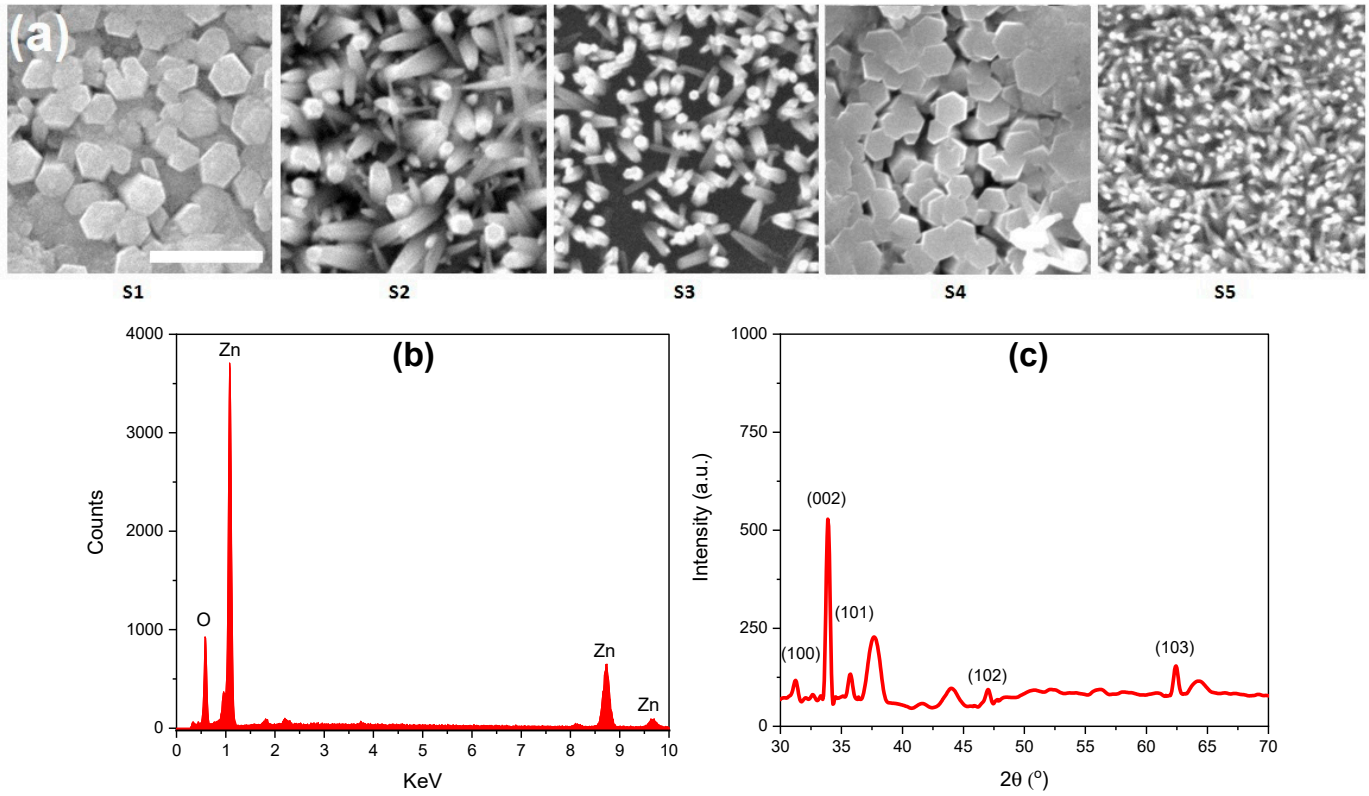

Figure 1. (**a**) Morphology of the grown ZnO nanorods samples at different precursor concentrations (scale bar = 2 μm), (**b**) EDX compositional analysis of the grown ZnO nanorods sample, and (**c**) XRD patterns of the grown ZnO nanorods.

The reaction of HMTA ($C_6H_{12}N_4$) with water at 80° (in 3 and 4) releases more OH^- ions. Therefore, in increased HMTA concentration conditions, the presence of excessive OH^- ions is expected. This high concentration of OH^- ions reduces the growth rate of ZnO nanorods and may also lead to their dissolution [32]. Moreover, the good or poor alignment of the nanorods and their growth density, as observed in Figure 1, can be related to the availability of the zinc precursor in the solution. At a low zinc nitrate/HMTA molar ratio, the zinc precursor can be depleted faster than OH^- ions, which leaves the growth solution with a high OH^- concentration and, therefore, a high possibility of nanorods eroding, leading to a subsequent deterioration of their alignment quality and vice versa [33,34].

The observed changes in the morphology of the grown ZnO nanorods can be explained based on the growth and erosion competition mechanism implemented during the growth process of the nanorods [35]. The polar (0002) facet of ZnO nanorods in the direction of the c-axis has greater ability to attract the available OH^- in the growth solution in comparison with the more stable non-polar side facets. Therefore, the top facet is more susceptible to growth and eroding. At a low OH^- concentration, the growth rate surpasses the erosion rate, and nanorods with enhanced dimensions are produced. In contrast, the erosion rate becomes greater than the growth rate at a high OH^- concentration, as the excessive OH^- ions participate in the eroding of the nanorods, resulting in the growth of nanorods with

reduced dimensions. The eroding process of the nanorods in the presence of excessive OH^- can be described through the following reactions [35]:

$$ZnO + OH^- \rightarrow ZnO_2^{2-} + H_2O \quad (7)$$

Figure 1b also shows the energy-dispersive X-ray (EDX) spectra of the grown samples, which indicates the presence of the elements zinc and oxygen and confirms the growth of pure ZnO nanostructures. The analysis of the grown samples composite shows an interesting variation in the atomic ratio of both elements in the samples. The ratios of Zn to O are 78.7:21.3, 79:21, 69.4:30.6, 71.6:28.4, and 79:21 for the samples S1, S2, S3, S4, and S5, respectively. The XRD patterns of the grown nanorods sample are shown in Figure 1c. The figure presents the main diffraction peaks (100), (002), (101), (102), and (103) of the hexagonal crystalline ZnO nanorods with preferential growth along the (002) direction (card no. 96-900-4179) [28]. Some additional peaks related to the gold layer can also be seen in the figure.

Figure 2 shows the absorption spectra of the MB-contaminated water samples in the presence of nanorods samples and at different UV irradiation times. The typical absorption peak of MB can be seen in Figure 2 at a wavelength value of about 664 nm. It can be seen clearly from the figure that all the samples are photocatalytically active, as the intensity of the main MB absorption peak intensity decreases with the increase in the UV irradiation time, but with varying activity levels. Samples S1, S4, and S5 show almost the same photocatalytic performance and are less active in comparison with samples S2 and S3. However, S3 shows the highest activity among the nanorods samples, as clearly shown by the absorption spectrum of the sample at 225 min with reduced MB peak intensity. An improvement in the MB degradation efficiency of about 122% was achieved for S3 in comparison with other samples; this was achieved by controlling the precursors' concentrations. Figure 3a–d summarizes the photocatalytic performance of the prepared ZnO nanorods samples. The reduction in the concentration of MB with various UV irradiation times for the various nanorods samples is shown in Figure 3a. As seen in the figure, all samples show reductions in MB concentration (C/C_o) with the irradiation time to different extents. At the maximum irradiation time (225 min), samples S1, S4, and S5 show a reduction in the MB concentration to about 90% of its initial value. Furthermore, the irradiation of sample S2 reduces the MB concentration to about 85% and a maximum reduction to about 75% can be seen for sample S3. These observations are supported by degradation efficiency calculations (DE % = $|(C_o - C)/C_o| \times 100 = |(A_o - A)/A_o| \times 100$) presented in Figure 3b, where C is the concentration of MB and A is the absorbance [12,36]. As seen in the figure, samples S1, S4, and S5 exhibit a degradation efficiency of about 10% at the highest irradiation time, while samples S2 and S3 show better performance with degradation efficiency of about 15% and 25%, respectively. This variation in the performance of the samples indicates that the concentration of the used precursors and their ratio has a significant influence on the morphological properties of the grown nanorods, as seen from the SEM images above, and their photocatalytic performance.

The reaction constant in each case was obtained based on the linear relation between $-ln\frac{C}{C_o}$ and the irradiation time, as shown in Figure 3c, where the constant k represents the slope of the line. It is clear from the figure that samples S1, S4, and S5 have similar slopes (reaction constants), whereas samples S2 and S3 have higher slopes (reaction constants). The values of the reaction constant for the various nanorods samples are shown in Figure 3d. It is clear from the figure that sample S3, which has a molar ration of zinc nitrate to HMTA equal to unity, has the highest reaction constant values among the prepared samples. The order of the prepared nanorods samples in terms of their photocatalytic activity from the highest to the lowest can be given as S3 > S2 > S4 > S1 > S5. Interestingly, this indicates that the samples with too-high and too-low zinc nitrate to HMTA ratios (i.e., S1 with a ratio of 2.00 and S5 with a ratio of 0.50) show the lowest photocatalytic activity. Therefore, based on these observations, it can be concluded that the precursors concentration and their ratio are very important parameters that can be utilized to tune the photocatalytic

performance of ZnO nanorods for water-treatment applications. The observed variation in the photocatalytic activity of ZnO nanorods samples has also been observed and discussed by other researchers investigating ZnO nanostructures. Such variation in the photocatalytic activity depends on many factors, mainly the morphology of the ZnO nanostructures, their surface area, their surface to volume ratio and, more importantly, the surface defects present [10,11]. The surface defects, such as oxygen vacancies and oxygen interstitials, which are considered the active sites for the photocatalytic processes, can potentially reduce the recombination of the photogenerated holes and electrons and thus effectively enhance the photocatalytic activity. Therefore, with the use of different molarity ratios and based on the observed variation in the samples' morphology and composition, the observed variation in their photocatalytic performance is definitely justified.

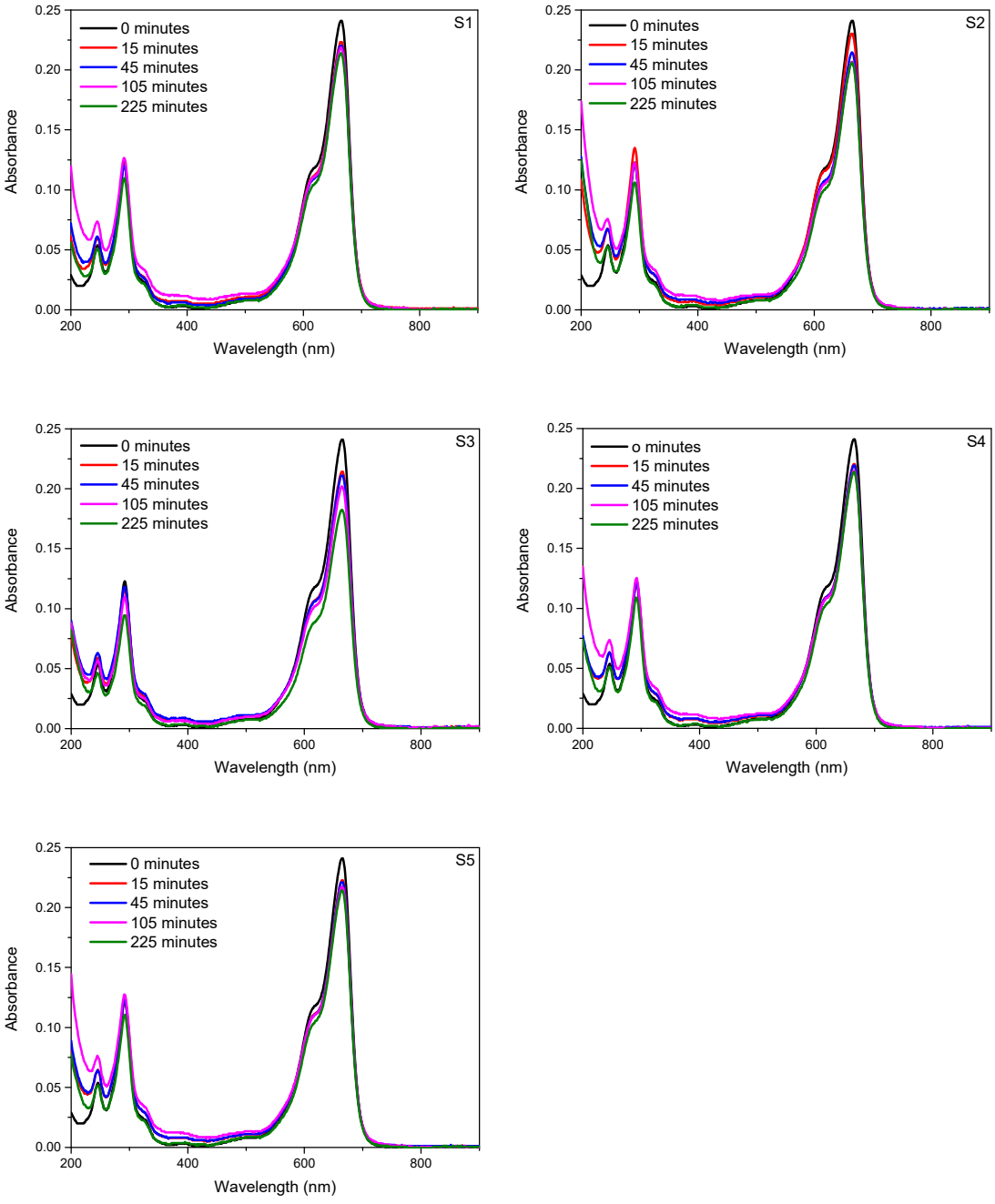

Figure 2. Absorption spectra of MB-polluted water samples in the presence of ZnO nanorods and at different UV irradiation times.

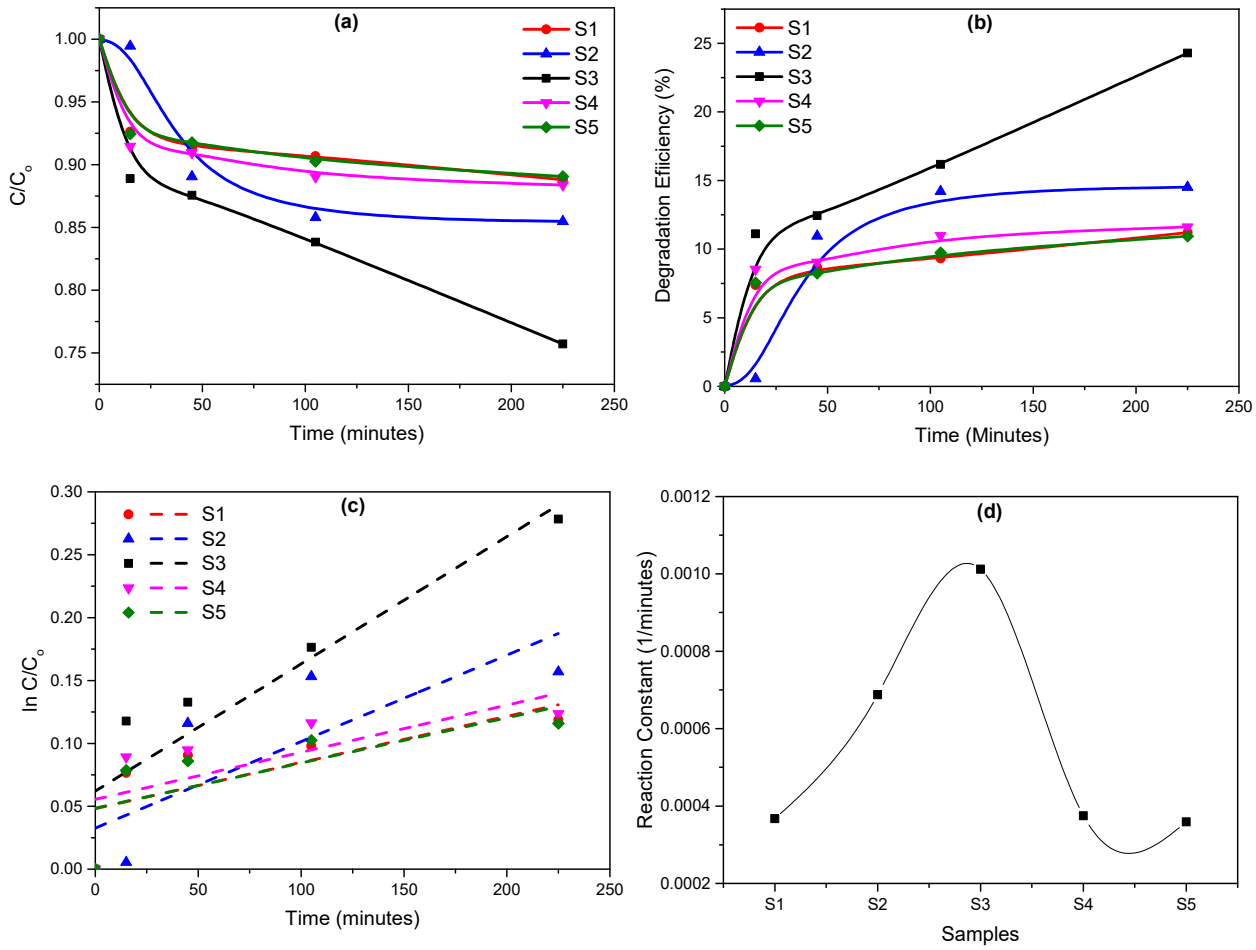

Figure 3. Photocatalytic performance of ZnO samples (**a**) MB concentration as a function of time, (**b**) degradation efficiency vs. time, (**c**) ln C/C_o vs. time, and (**d**) reaction constant of the different samples.

Figure 4 shows the variation in the performance of ZnO nanorods over a period of 60 days. The nanorods samples were kept in polluted water and their MB degradation performance was evaluated directly after their synthesis, after 30 days, and after 60 days. As seen in Figure 4a, there was an obvious degradation in the performance of the nanorods with the time the samples were kept in the polluted aqueous environment. Moreover, the observed degradation differed from one sample to another, which can be related to their preparation condition and their morphology as well. The reduction in the photocatalytic performance was similar for samples S1, S4, and S5, while less reduction was observed for samples S2 and S3. Figure 4b shows the performance degradation percentage after 30 days and 60 days. It can be seen from the figure that the degradation in the samples' performance is in the range of 35–48% in the first 30 days and reaches more than 80% after 60 days. However, the degradation in the case of samples S1, S4, and S5 is more severe (~80%) than that for samples S2 and S3, which experienced a performance degradation percentage of about 53% only after 60 days of being kept in a polluted aqueous environment. The degradation rate of the nanorods samples over a period of 60 days in an aqueous environment is shown in Figure 4c.

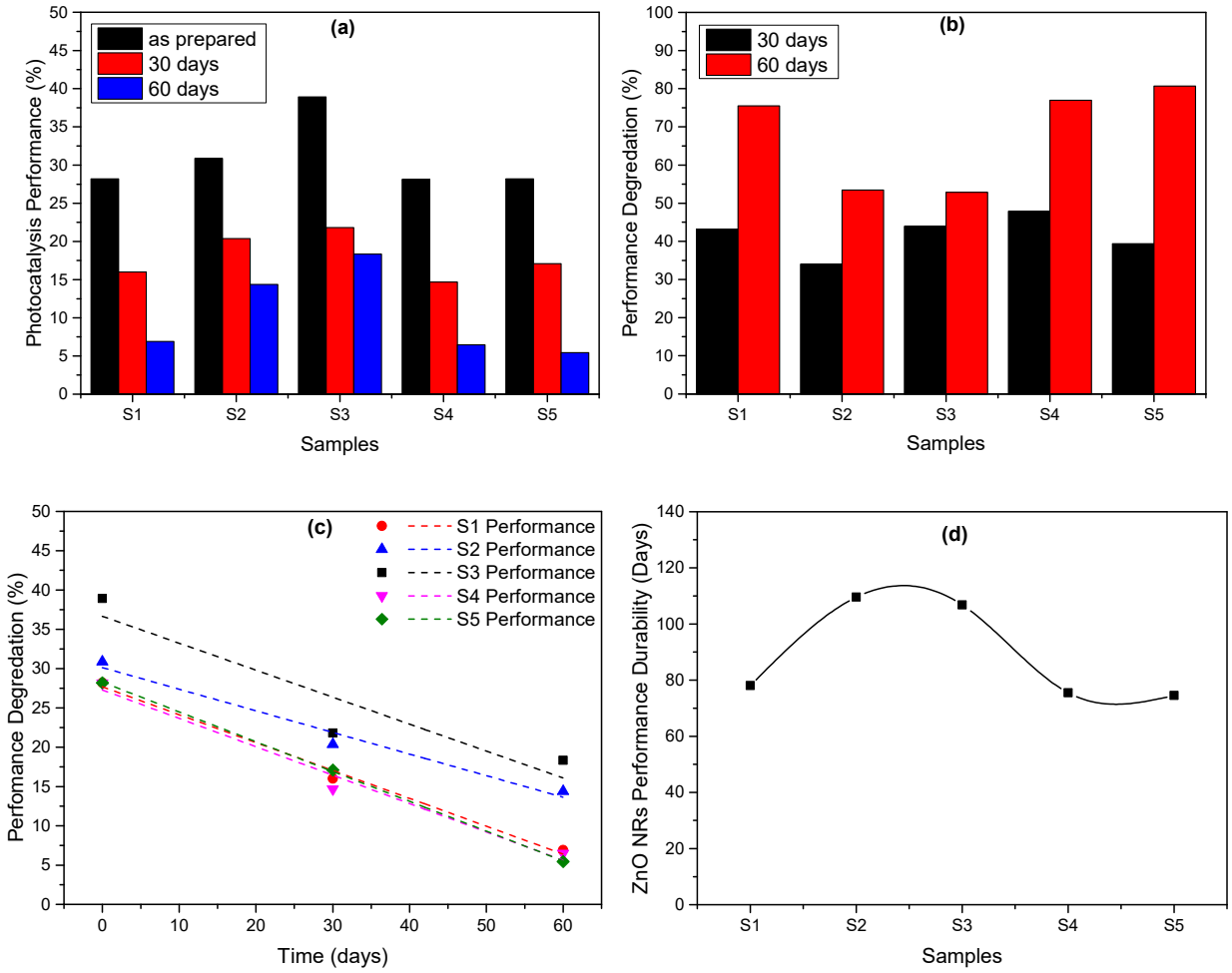

Figure 4. Photocatalytic performance variation of ZnO samples (**a**) performance degradation over a period of 60 days, (**b**) performance degradation percentage, (**c**) performance degradation rate, (**d**) performance durability.

The degradation rate of each sample was estimated based on the slope of the linear fitting of the data. Samples S1, S4, and S5 exhibited higher degradation rates than samples S2 and S3. Moreover, sample S2 showed a lower degradation rate than sample S3. Based on these data, the performance durability of the nanorods samples was estimated. The estimation results are presented in Figure 4d and show that sample S2 is the most durable sample, as it can remain photocatalytically active for about 110 days. Then, sample S3 comes second in terms of photocatalytic activity with a photocatalytic activity period of about 106 days, followed by S1, S4, and S5 with activity periods of 78, 76, and 75 days, respectively. These results clearly indicate that the ratio of the precursors used to prepare ZnO nanorods not only affects the photocatalytic performance of the nanorods sample but also plays a key role in determining the amount of time for which the nanorods remain photocatalytically active in aqueous environments. As seen from the figure and the analysis above, an increase in the photocatalytic activity time of the nanorods sample of approximately 47% ($[TS2 - TS5/TS5] \times 100$) can be achieved easily by varying the precursors ratio, which would have a great impact on the use of these nanomaterials and the related economic aspects for water-treatment applications.

In addition to the nanorods samples performance evaluation and their performance durability, the variation in the morphology of the nanorods samples was investigated by imaging the nanorods samples directly after their synthesis, directly after they were first used for water treatment (0 days in water), after their second use for water treatment (after 30 days in water), and after their third use for water treatment (after 60 days in water) as

shown in Figure 5. It is clear from the figure that the prepared samples had different abilities in terms of retaining their initial morphology after being kept in an aqueous environment for 60 days. It can be seen from the figure that some samples experienced a high level of corrosion/damage while others were affected to a minimal degree.

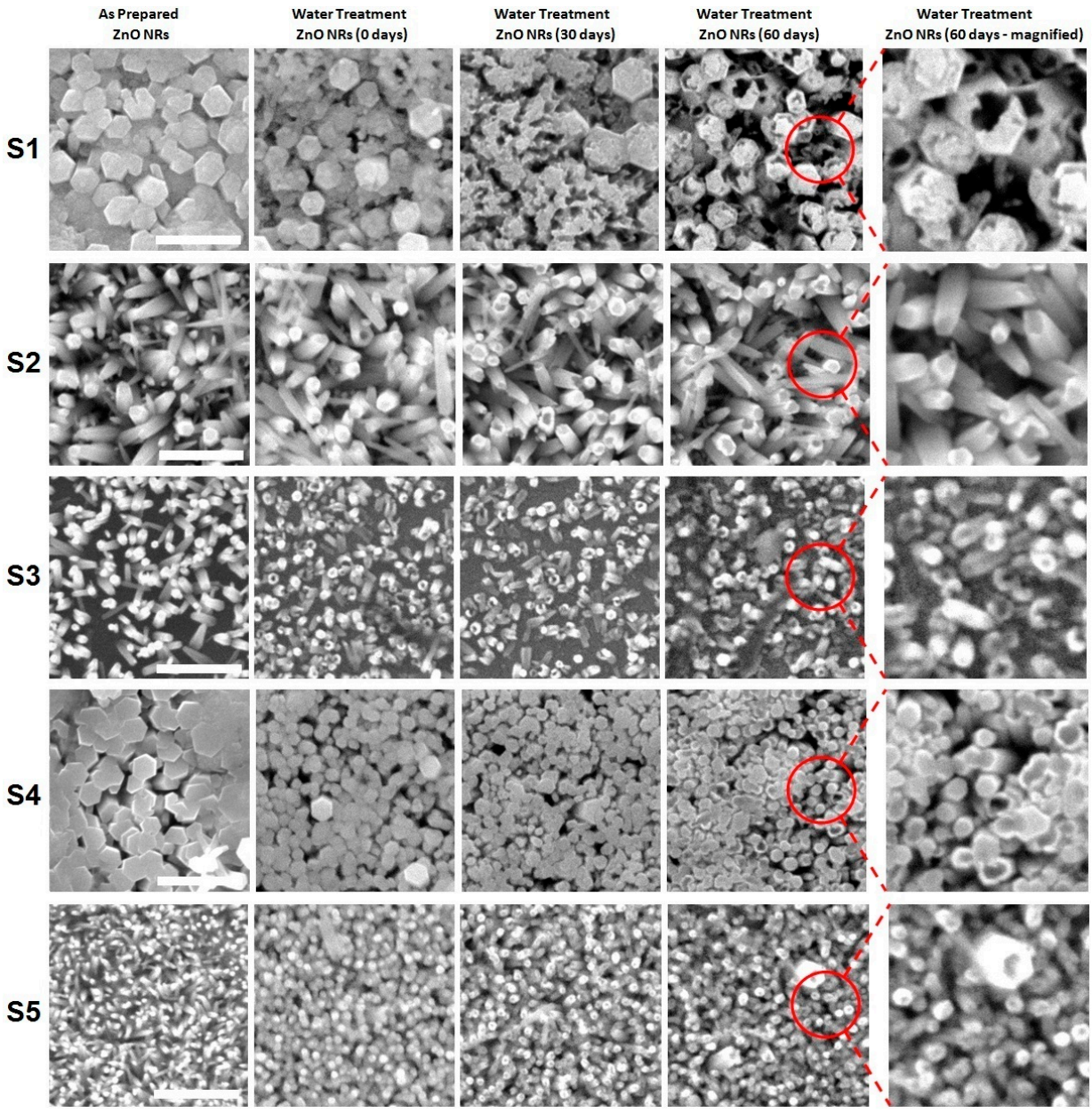

Figure 5. Variation in ZnO nanorods samples' morphology (scale bar = 2 μm): as prepared (first column from left), after first water treatment (second column), after second water treatment (30 days in water—third column), after third water treatment (60 days in water—fourth column and magnified images—fifth column).

For example, in the case of sample S1, severe erosion of the nanorods took place after the nanorods had been kept in water for 30 and 60 days. It also seems that the erosion started at the sides of the nanorods. The same observations can be seen for sample S2, but with less severity. Samples S4 and S5 also exhibited similar erosion behavior, with more erosion occurring in sample S4 in comparison with sample S5. It also appears that the erosion affected the top facet of the nanorods more than their side facets. Sample S3 also experienced a moderate erosion of both the top and side facets, as well as a morphological

transformation from nanorods to nanotubes. In general, dissolving MB in water results in a low-pH acidic solution with a pH value in the range of 5–6 [37–39]. In such an acidic environment, ZnO nanorods usually erode and their different facets start to dissolve at different degrees [40–44]. Therefore, as the nanorods samples were kept in MB-polluted water with low pH value, the observed erosion that occurred in the nanorod samples was expected. However, the change in the erosion behavior from one sample to another one based was very interesting and was completely attributed to the used precursors ratios. Another interesting observation is that although some studies have reported that the erosion of the [0001] polar facet in the acidic environment was the fastest in comparison with the {0110} non-polar facets, the SEM images in Figure 6 show that the erosion behavior may depend on the sample and its preparation conditions, as discussed above [43,45].

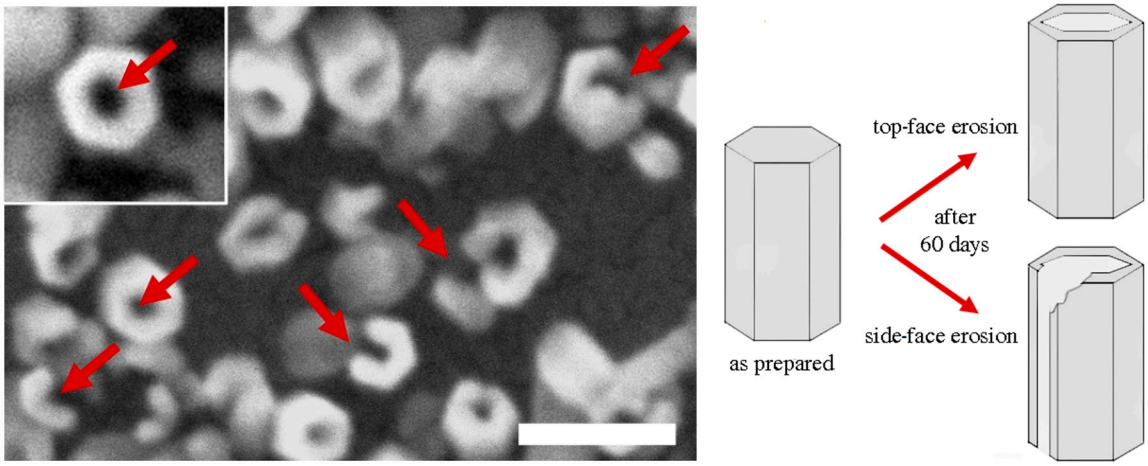

Figure 6. Morphology of ZnO nanorods in the sample S3 after 60 days in MB polluted water: SEM image (**left**—scale bar = 500 nm) and illustrating sketch (**right**).

To relate the observed variation in the samples' morphology and their performance durability, Figure 6 presents the SEM images of sample S3 after it was kept in polluted water for 60 days. Sample S3 showed the best photocatalytic performance and lowest performance degradation over the period of the study. This can be explained based on the observed variation in the sample morphology.

The erosion of the nanorods in this sample gradually converts them to nanotubes, as seen from the SEM images. Therefore, the degradation in the performance of the nanorods is partially compensated by the continuous increase in the nanorods' surface area due to the exposure of more inner parts of the nanorod during the transformation process. This results in less performance degradation for sample S3 over the study period in comparison with other samples in which less erosion effects and/or damage to the nanorods occur. Exposure of the inner parts of ZnO nanorods through their morphological transformation from rods to tubes has been found to enhance their performance in gas-sensing applications, as reported in [46]. Table 2 shows a comparison of the achieved enhancement in MB degradation as reported in different studies. The reduced degradation effects and the good photocatalytic performance of sample S3 were achieved by varying the precursors ratios, which indicates that the photocatalytic performance, performance degradation, and photocatalytic activity duration can be tuned easily for ZnO nanorods by controlling the growth conditions. This would also open the door for further research focused on investigating the effect of other growth conditions, such as wider range of precursors molarities, growth temperature, growth time, post-annealing/treatment, applied potential, and other possible process parameters.

Table 2. Comparison of the achieved enhancement in MB degradation reported in different studies.

Sample	Growth Method	Optimization Parameter	Achieved Enhancement in MB Degradation	Reference
ZnO NRs	Hydrothermal	Seed layer	50%	[47]
ZnO NRs	Hydrothermal	Seed layer	16.25%	[48]
ZnO NRs	Laser ablation/ Hydrothermal	pH	13.26%	[49]
ZnO NRs	sol–gel/ Hydrothermal	ZnO dosage	46%	[50]
ZnO NRs	sol–gel	Coated layers	74.5%	[51]
ZnO NRs	Electrodeposition	Precursors concentration ratio	122%	This work

4. Conclusions

Successful growth of ZnO nanorods on sputtered Au layers via a low-cost electrodeposition technique was achieved. The molar ratio of the used precursors was varied and its effect on the morphology and photocatalytic activity of the prepared nanorods for water-treatment applications was investigated. The grown nanorods exhibited different dimensions and different photocatalytic activities as well. They also showed different capabilities to maintain their initial morphology after prolonged time spent in an aqueous environment. Interestingly, of the molarity and molarity ratios (ZN/HMTA) used, the sample with a precursor molarity ratio of unity showed the highest photocatalytic activity and the lowest performance degradation ratio after being kept in polluted water for 60 days. Moreover, the sample with a precursors ratio slightly less than unity remained photocatalytically active for a longer time than other samples, which can be attributed to the good ability of the sample to retain its morphology and, hence, the available photoactive surface. The findings clearly show that utilizing this growth parameter, the precursors ratio, could lead to significant improvements in the activity and the performance durability of ZnO nanorods for water-treatment applications and will also positively impact their industrial-related economic aspects. Moreover, these findings will form the basis for many future studies on maximizing the performance efficiency of ZnO nanorods and, most importantly, their durability, especially in a vital field such as water purification, via controlling the various growth parameters, use of post-treatments, and coatings.

Author Contributions: A.S.A.: conceptualization, methodology, visualization, formal analysis, investigation, writing—original draft; M.M.: methodology, investigation, formal analysis, writing—review and editing; Z.R.K.: methodology, writing—review and editing; M.B.: methodology, investigation, writing—review and editing, M.G.: methodology, writing—review and editing. All authors have read and agreed to the published version of the manuscript.

Funding: This work is supported by the Deanship of Scientific Research at the University of Hail, Saudi Arabia, through project number <<RG-23057>>.

Data Availability Statement: The data presented in this study are available from the corresponding author upon reasonable request.

Conflicts of Interest: The authors declare no conflicts of interest.

References

1. Khin, M.M.; Nair, A.; Babu, V.; Murugan, R.; Ramakrishna, S. A review on nanomaterials for environmental remediation. *Energy Environ. Sci.* **2012**, *5*, 8075–8109. [CrossRef]
2. Perreault, F.; De Faria, A.F.; Elimelech, M. Environmental applications of graphene-based nanomaterials. *Chem. Soc. Rev.* **2015**, *44*, 5861–5896. [CrossRef]
3. Ghasemzadeh, G.; Momenpour, M.; Omidi, F.; Hosseini, M.; Ahani, M.; Barzegari, A. Applications of nanomaterials in water treatment and environmental remediation. *Front. Environ. Sci. Eng.* **2014**, *8*, 471–482. [CrossRef]
4. Alshammari, A.S.; Alenezi, M.R.; Lai, K.T.; Silva, S.R.P. Inkjet printing of polymer functionalized CNT gas sensor with enhanced sensing properties. *Mater. Lett.* **2017**, *189*, 299–302. [CrossRef]

5. Shan, G.; Surampalli, R.Y.; Tyagi, R.D.; Zhang, T.C. Nanomaterials for environmental burden reduction, waste treatment, and nonpoint source pollution control: A review. *Front. Environ. Sci. Eng. China* **2009**, *3*, 249–264. [CrossRef]
6. Yang, L.; Yang, L.; Ding, L.; Deng, F.; Luo, X.; Luo, S. Principles for the application of nanomaterials in environmental pollution control and resource reutilization. In *Nanomaterials for the Removal of Pollutants and Resource Reutilization*; Elsevier: Amsterdam, The Netherlands, 2019; pp. 1–23.
7. Muruganandham, M.; Zhang, Y.; Suri, R.; Lee, G.; Chen, P.; Hsieh, S.; Sillanpyää, M.; Wu, J.J. Environmental applications of ZnO materials. *J. Nanosci. Nanotechnol.* **2015**, *15*, 6900–6913. [CrossRef] [PubMed]
8. Guo, Y.; Zhang, Y.; Li, T.; Tao, T. ZnO quantum dots for fluorescent detection of environmental contaminants. *J. Environ. Chem. Eng.* **2021**, *9*, 106800. [CrossRef]
9. Yuan, Y.; Huang, G.; Hu, W.; Xiong, D.; Huang, W. Tunable synthesis of various ZnO architectural structures with enhanced photocatalytic activities. *Mater. Lett.* **2016**, *175*, 68–71. [CrossRef]
10. Xu, F.; Shen, Y.; Sun, L.; Zeng, H.; Lu, Y. Enhanced photocatalytic activity of hierarchical ZnO nanoplate-nanowire architecture as environmentally safe and facilely recyclable photocatalyst. *Nanoscale* **2011**, *3*, 5020–5025. [CrossRef]
11. Udom, I.; Ram, M.K.; Stefanakos, E.K.; Hepp, A.F.; Goswami, D.Y. One dimensional-ZnO nanostructures: Synthesis, properties and environmental applications. *Mater. Sci. Semicond. Process.* **2013**, *16*, 2070–2083. [CrossRef]
12. Mohamed, M.; Alshammari, A.S.; Almokhtar, M. Structure, morphology and photocatalytic activity of ZnO nanorods fabricated by electrochemical deposition. *Appl. Phys. A* **2020**, *126*, 1–8. [CrossRef]
13. Kuo, T.-J.; Lin, C.; Kuo, C.; Huang, M.H. Growth of ultralong ZnO nanowires on silicon substrates by vapor transport and their use as recyclable photocatalysts. *Chem. Mater.* **2007**, *19*, 5143–5147. [CrossRef]
14. Das, J.; Khushalani, D. Nonhydrolytic route for synthesis of ZnO and its use as a recyclable photocatalyst. *J. Phys. Chem. C* **2010**, *114*, 2544–2550. [CrossRef]
15. Limón-Rocha, I.; Guzmán-González, C.A.; Anaya-Esparza, L.M.; Romero-Toledo, R.; Rico, J.L.; González-Vargas, O.A.; Pérez-Larios, A. Effect of the Precursor on the Synthesis of ZnO and Its Photocatalytic Activity. *Inorganics* **2022**, *10*, 16. [CrossRef]
16. Rodríguez-Flores, T.; Haro-Pérez, C.; Gerardo-Morales, E.E.; Huerta-Hernández, G.E.; González-Reyes, L.; Hernández-Pérez, I. Influence of Precursor Concentration in the Synthesis of ZnO Nanoparticles on their Morphological, Structural, and Photocatalytic Properties. *Top. Catal.* **2022**, *65*, 1149. [CrossRef]
17. Zhang, X.; Qin, L.; Xue, Y.; Yu, P.; Zhang, B.; Wang, L.; Liu, R. Effect of aspect ratio and surface defects on the photocatalytic activity of ZnO nanorods. *Sci. Rep.* **2014**, *4*, 4596. [CrossRef] [PubMed]
18. Liu, Y.; Kang, Z.H.; Chen, Z.H.; Shafiq, I.; Zapien, J.A.; Bello, I.; Zhang, W.J.; Lee, S.T. Synthesis, characterization, and photocatalytic application of different ZnO nanostructures in array configurations. *Cryst. Growth Des.* **2009**, *9*, 3222. [CrossRef]
19. Ong, C.B.; Ng, L.Y.; Mohammad, A. A review of ZnO nanoparticles as solar photocatalysts: Synthesis, mechanisms and applications. *Renew. Sustain. Energy Rev.* **2018**, *81*, 536. [CrossRef]
20. Li, X.; Zhang, B.; Wu, Q.; Zhang, C.; Yu, Y.; Li, Y.; Lin, W.; Cheng, H.; Zhao, F. A facile strategy for confining ZnPd nanoparticles into a ZnO@ Al_2O_3 support: A stable catalyst for glycerol hydrogenolysis. *J. Catal.* **2016**, *337*, 284–292. [CrossRef]
21. İkizler, B.; Peker, S. Stability of ZnO nanorods coated on the channel wall under continuous flow conditions. *Adv. Mater. Lett.* **2014**, *5*, 325–332. [CrossRef]
22. Manthina, V.; Agrios, A.G. Single-pot ZnO nanostructure synthesis by chemical bath deposition and their applications. *Nano-Struct. Nano-Objects* **2016**, *7*, 1–11. [CrossRef]
23. Sun, X.; Chen, X.; Deng, Z.X.; Li, Y.D. A CTAB-assisted hydrothermal orientation growth of ZnO nanorods. *Mater. Chem. Phys.* **2003**, *78*, 99–104. [CrossRef]
24. Chen, Z.; Gao, L. A new route toward ZnO hollow spheres by a base-erosion mechanism. *Cryst. Growth Des.* **2008**, *8*, 460–464. [CrossRef]
25. Liu, X.; Jin, Z.; Liu, Z.; Yu, K.; Bu, S. Nanostructured ZnO films obtained by a basic erosion method. *Appl. Surf. Sci.* **2006**, *252*, 8668–8672. [CrossRef]
26. Yin, Z.; Wang, Z.; Du, Y.; Qi, X.; Huang, Y.; Xue, C.; Zhang, H. Full solution-processed synthesis of all metal oxide-based tree-like heterostructures on fluorine-doped tin oxide for water splitting. *Adv. Mater.* **2012**, *24*, 5374–5378. [CrossRef]
27. Sun, X.; Li, Q.; Jiang, J.; Mao, Y. Morphology-tunable synthesis of ZnO nanoforest and its photoelectrochemical performance. *Nanoscale* **2014**, *6*, 8769–8780. [CrossRef] [PubMed]
28. Skompska, M.; Zarebska, K. Electrodeposition of ZnO Nanorod Arrays on Transparent Conducting Substrates—A Review. *Electrochim. Acta* **2014**, *127*, 467–488. [CrossRef]
29. Parize, R.; Garnier, J.; Chaix-Pluchery, O.; Verrier, C.; Appert, E.; Consonni, V. Effects of hexamethylenetetramine on the nucleation and radial growth of ZnO nanowires by chemical bath deposition. *J. Phys. Chem. C* **2016**, *120*, 5242–5250. [CrossRef]
30. McPeak, K.M.; Le, T.P.; Britton, N.G.; Nickolov, Z.S.; Elabd, Y.A.; Baxter, J.B. Chemical bath deposition of ZnO nanowires at near-neutral pH conditions without hexamethylenetetramine (HMTA): Understanding the role of HMTA in ZnO nanowire growth. *Langmuir* **2011**, *27*, 3672–3677. [CrossRef]
31. Wang, S.F.; Tseng, T.Y.; Wang, Y.R.; Wang, C.Y.; Lu, H.C.; Shih, W.L. Effects of preparation conditions on the growth of ZnO nanorod arrays using aqueous solution method. *Int. J. Appl. Ceram. Technol.* **2008**, *5*, 419–429. [CrossRef]

32. Kim, D.; Leem, J.-Y. Effect of the pH of an aqueous solution on the structural, optical, and photoresponse properties of hydrothermally grown ZnO nanorods and the fabrication of a high performance ultraviolet sensor. *J. Korean Phys. Soc.* **2018**, *72*, 400–405. [CrossRef]
33. Tian, J.-H.; Hu, J.; Li, S.S.; Zhang, F.; Liu, J.; Shi, J.; Li, X.; Tian, Z.Q.; Chen, Y. Improved seedless hydrothermal synthesis of dense and ultralong ZnO nanowires. *Nanotechnology* **2011**, *22*, 245601. [CrossRef] [PubMed]
34. Saha, R.; Saha, N.R.; Karmakar, A.; Dalapati, G.K.; Chattopadhyay, S. Generation of oxygen interstitials with excess in situ Ga doping in chemical bath deposition process for the growth of p-type ZnO nanowires. *J. Mater. Sci. Mater. Electron.* **2019**, *30*, 8796–8804. [CrossRef]
35. Kim, K.S.; Jeong, H.; Jeong, M.S.; Jung, J.Y. Polymer-templated hydrothermal growth of vertically aligned single-crystal ZnO nanorods and morphological transformations using structural polarity. *Adv. Funct. Mater.* **2010**, *20*, 3055–3063. [CrossRef]
36. Mohamed, M.; Alfatah, A.A.; Alshammari, A.S. Structure, linear and nonlinear optical and photocatalytic properties investigation of ZnO nanorods: Influence of growth time. *J. Mater. Sci. Mater. Electron.* **2023**, *34*, 446. [CrossRef]
37. Galenda, A.; Natile, M.M.; El Habra, N. Large-Scale MOCVD Deposition of Nanostructured TiO_2 on Stainless Steel Woven: A Systematic Investigation of Photoactivity as a Function of Film Thickness. *Nanomaterials* **2022**, *12*, 992. [CrossRef] [PubMed]
38. Soltani, N.; Saion, E.; Yunus, W.M.M.; Navasery, M.; Bahmanrokh, G.; Erfani, M.; Zare, M.R.; Gharibshahi, E. Photocatalytic degradation of methylene blue under visible light using PVP-capped ZnS and CdS nanoparticles. *Solar Energy* **2013**, *97*, 147–154. [CrossRef]
39. Zhang, D.; Wang, Q.; Wang, L.; Zhang, L. Magnetically separable $CdFe_2O_4$/graphene catalyst and its enhanced photocatalytic properties. *J. Mater. Chem. A* **2015**, *3*, 3576–3585. [CrossRef]
40. Baruah, S.; Dutta, J. pH-dependent growth of zinc oxide nanorods. *J. Cryst. Growth* **2009**, *311*, 2549–2554. [CrossRef]
41. Shin, C.; Heo, J.H.; Jeong, Y.I.; Oh, H.B.; Ryu, H.; Lee, W.J.; Chang, J.H.; Kim, J.H.; Choi, H. Structural and optical properties of hydrothermally grown zinc oxide nanorods on polyethersulfone substrates as a function of the growth temperature and duration. *Thin Solid Film.* **2012**, *520*, 2449–2454. [CrossRef]
42. Shirzad-Siboni, M.; Jonidi-Jafari, A.; Farzadkia, M.; Esrafili, A.; Gholami, M. Enhancement of photocatalytic activity of Cu-doped ZnO nanorods for the degradation of an insecticide: Kinetics and reaction pathways. *J. Environ. Manag.* **2017**, *186*, 1–11. [CrossRef] [PubMed]
43. Lin, C.-H.; Cheng, S.Y.; Lin, R.J.; Wang, Y.H. Manipulation of ZnO nanowire by low-temperature solution approach. *MRS Online Proc. Libr.* **2005**, *891*, 0891-EE10-21. [CrossRef]
44. Rafaie, H.; Samat, N.; Nor, R.M. Effect of pH on the growth of zinc oxide nanorods using Citrus aurantifolia extracts. *Mater. Lett.* **2014**, *137*, 297–299. [CrossRef]
45. Tsai, M.; Huang, C.C.; Lee, Y.C.; Yang, C.S.; Yu, H.C.; Lee, J.W.; Hu, S.Y.; Chen, C.H. A study on morphology control and optical properties of ZnO nanorods synthesized by microwave heating. *J. Lumin.* **2012**, *132*, 226–230. [CrossRef]
46. Fulati, A.; Usman Ali, S.M.; Riaz, M.; Amin, G.; Nur, O.; Willander, M. Miniaturized pH sensors based on zinc oxide nanotubes/nanorods. *Sensors* **2009**, *9*, 8911–8923. [CrossRef] [PubMed]
47. Bourfaa, F.; Boutelala, A.; Aida, M.S.; Attaf, N.; Ocak, Y.S. Influence of Seed Layer Surface Position on Morphology and Photocatalysis Efficiency of ZnO Nanorods and Nanoflowers. *J. Nanomater.* **2020**, *2020*, 4072351. [CrossRef]
48. Dash, P.; Manna, A.; Mishra, N.C.; Varma, S. Synthesis and characterization of aligned ZnO nanorods for visible light photocatalysis. *Phys. E* **2019**, *107*, 38–46. [CrossRef]
49. Abbas, K.; Bidin, N. Morphological driven photocatalytic activity of ZnO nanostructures. *Appl. Surf. Sci.* **2017**, *394*, 498–508. [CrossRef]
50. Luo, S.; Liu, C.; Wan, Y.; Li, W.; Ma, C.; Liu, S.; Heeres, H.J.; Zheng, W.; Seshan, K.; He, S. Self-assembly of single-crystal ZnO nanorod arrays on flexible activated carbon fibers substrates and the superior photocatalytic degradation activity. *Appl. Surf. Sci.* **2020**, *513*, 145878. [CrossRef]
51. Xu, L.; Xian, F.; Pei, S.; Zhu, Y. Photocatalytic degradation of organic dyes using ZnO nanorods supported by stainless steel wire mesh deposited by one-step method. *Optik* **2020**, *203*, 164036. [CrossRef]